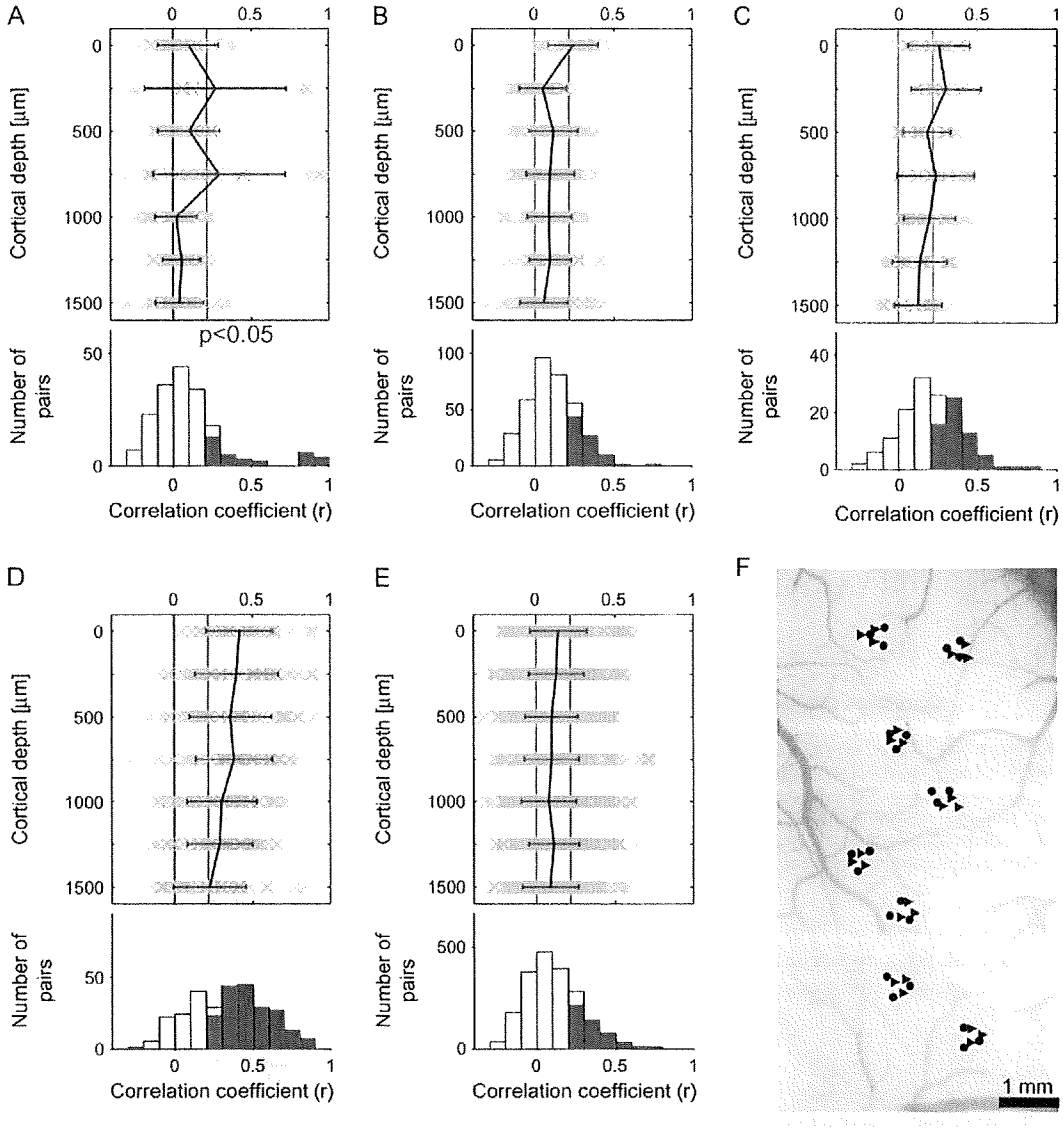

Figure 15. Similarity in stimulus selectivity between single isolated cells, MUs, and between single isolated cells and averaged MUs in hemisphere H2, where recording sites were randomly chosen without the guidance of intrinsic signal imaging. (*A*, *B*, *C*) correspond to Figures 6(*Aa*,*Ba*), (*Ab*,*Bb*), and (*Ac*,*Bc*), respectively. Conventions are the same as in Figure 6. (*D*, *E*) correspond to Figures 7(*Aa*,*Ba*) and (*Ab*,*Bb*), respectively. Conventions are the same as in Figure 7. (*F*) represents recording sites from hemisphere H2. Density of recordings within individual sites, and site-to-site distances, was adjusted nearly the same as in H1 and H3.

signal imaging. We addressed this issue by recording neuronal activities from another hemisphere (H2), in which we did not conduct intrinsic signal imaging beforehand but instead randomly chose 8 sites for extracellular recording (Fig. 15*F*). The results of the analysis of correlation among single cells, MUs, and averaged MUs for these sites were consistent with the results for the spots identified with intrinsic signal imaging and support the idea of the columnar organization in area TE: 1) the proportion of the pairs of a single neuron and the averaged MU with significant correlation (43.1%) was higher than the proportion of single-neuron pairs with significant correlation (18.1%) (Figs. 15*A*,*C*), 2) the correlation coefficient for the pairs of a single neuron and the averaged MU (0.20 ± 0.19, mean ± SD) were higher than that for the single-neuron pairs (0.10 ± 0.24), and 3) the proportion of pairs of an MU and the averaged MU with significant correlation, both within the same site, was as high as 65.7% (Fig. 15*D*), but the proportion was as low as 23.7% for pairs of an MU and the averaged MU at different sites (Fig. 15*E*). However, we found some tendency of the correlation being lower than that obtained from cells within the spots identified by intrinsic signal imaging. In particular, the proportion of MU pairs with significant correlation (22.7%) (Fig. 15*B*) was almost the same as the proportion of single-neuron pairs (18.1%) (Fig. 15*A*). This result was not due to the property specific to subpopulation of spots (Fig. 16). For the spots identified by intrinsic signal imaging (n = 9: 4 and 5 spots from H1 and H3, respectively), the distribution of spots shifted to the right (higher in values of the correlation coefficient) when MUs were used to calculate values of correlation coefficient (Fig. 16*A*). On the other hand, distribution did not show such shift for the randomly chosen sites (n = 8 from H2) (Fig. 16*B*). Based on this result, we

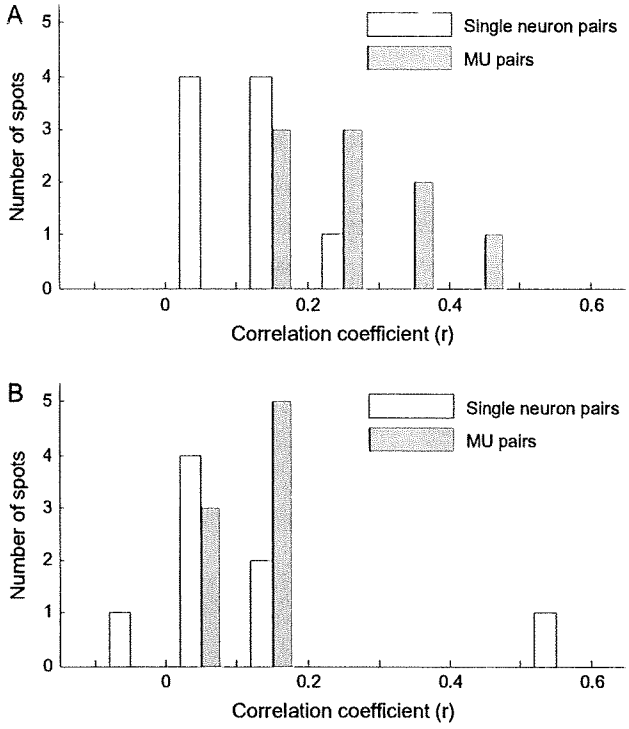

Figure 16. Relationship of object selectivity between single-neuron pairs and MU pairs for the spots identified by intrinsic signal imaging (*A*) and for the randomly chosen sites (*B*). The mean value of correlation coefficient (*r*) was calculated separately for each spot, and distribution of spots was plotted against the mean values of correlation coefficient. Total number of spots was 9 (4 spots from H1 and 5 spots from H3) for activity spots and 8 for randomly chosen sites.

suggest that IT cortex is organized in the region where neurons having similar response property are densely clustered and the region where those neurons are sparsely clustered (discussed later in detail).

Discussion

To examine the columnar organization in a cortical area, it is essential to use a set of stimuli that well characterizes functional properties of the cells in the area. However, such optimal stimulus sets are not available in many cortical areas, particularly in association cortices, and thus, firm evidence for columnar organizations is lacking in these areas. In the present study, we explored ways to examine columnar organizations in area TE without explicitly identifying the optimal stimulus set.

A general assumption is that because IT cortex is essential for object vision, evoked responses to a large number of object images should reflect functional properties of individual cells in IT cortex. On this basis, we examined selectivity of cells through their responses to 100 object images. We found that object selectivity is largely different from cell to cell, even if these cells are located in close vicinity (150 μm). However, this result does not eliminate the possibility of columnar organization in IT cortex. More importantly, we found that the selectivity of the averaged MU was similar to that of individual cells and MUs if they were recorded from the same spots (Figs 6*Ac*,*Bc* and 7*Aa*,*Ba*) but was different if cells and MUs were chosen from different spots (Fig. 7*Ab*,*Bb*). These results support the idea that a columnar organization does exist with respect to stimulus selectivity characterized by the averaged MUs.

The basis of the difference between cell-to-cell and cell-to-averaged MU similarity in object selectivity is well represented in tuning curves of individual cells where cells' evoked responses to object stimuli are plotted against the object stimuli arranged in the descending order of the preferred object images of the averaged MU (Fig. 17). Because there was cell-to-cell variability in object selectivity, different neurons had different peaks in the tuning curves. In most of the neurons, however, there was a general tendency that higher evoked responses were elicited by more effective object images for averaged MUs, and lower evoked responses were elicited by less effective object images for averaged MUs. These results could be explained by assuming that each neuron receives 2 different types of inputs: one specific for each neuron and the other common across the neurons within a spot (Fig. 18). The cell-specific inputs would be involved more in cell-specific responses to the object images that appeared as cell-specific peaks in the tuning curve, and the common inputs generate the general tendency of the tuning curve to be similar to that of averaged MUs. The cell-specific peaks in the individual tuning curves were different from cell to cell and were removed by averaging the MUs. Consequently, the common properties across the cells were disclosed in the averaged MUs (see also Appendix). The present study suggests that the common properties of a spot were different from those of the other spots if these spots were spaced at least 600 μm apart (Fig. 7*Ac*,*Bc*).Although common properties across the cells remained after averaging activities of MUs, it is possible that tuning specificity was greatly reduced by averaging and the averaged activities may lose stimulus selectivity that is meaningful for object image processing. To address this possibility, we calculated the sparseness index (SI) as a measure of tuning specificity for 80 object images (Rolls and Tovee, 1995). The SI is defined as

$$SI=\Big(\sum_{i=1}^{n} r_i/n\Big)^2 \Big/ \sum_{i=1}^{n} (r_i^2/n),$$

where r_i is the evoked response (spikes/s) to the ith stimulus in the set of n stimuli. It takes on a maximum value 1 if the all the stimuli activate the cell in identical evoked responses and takes $1/n$ if only one of n stimuli activates the cell. The SI of the evoked responses to the 80 object stimuli by single cells for H1 and H3 was, on average, 0.19 ± 0.18 (mean ± SD, n = 218). On the other hand, the SIs for MUs and averaged MUs for H1 and H3 were 0.33 ± 0.21 and 0.61 ± 0.18 (mean ± SD, n = 309 and 9 for MUs and averaged MUs, respectively). Thus, there was indeed a decrease in stimulus specificity. However, an SI of 0.6 is considered to be in the range indicating that the responses were still stimulus specific (Fig. 13; Rolls and Tovee 1995). The SIs calculated for the evoked responses of single cells, MUs, and averaged MUs in H2 were 0.17 ± 0.17 (n = 144), 0.17 ± 0.17 (n = 286), and 0.48 ± 0.20 (n = 8), respectively (mean ± SD).

The above discussion is based on the hemispheres where extracellular activities were recorded from activity spots that were predetermined by intrinsic signal imaging, and thus, the results may not reflect general properties of area TE. Here, we considered possible biases introduced by recording from specific sites in 2 aspects. First, because the stimuli used in intrinsic signal imaging were involved in 100 object images

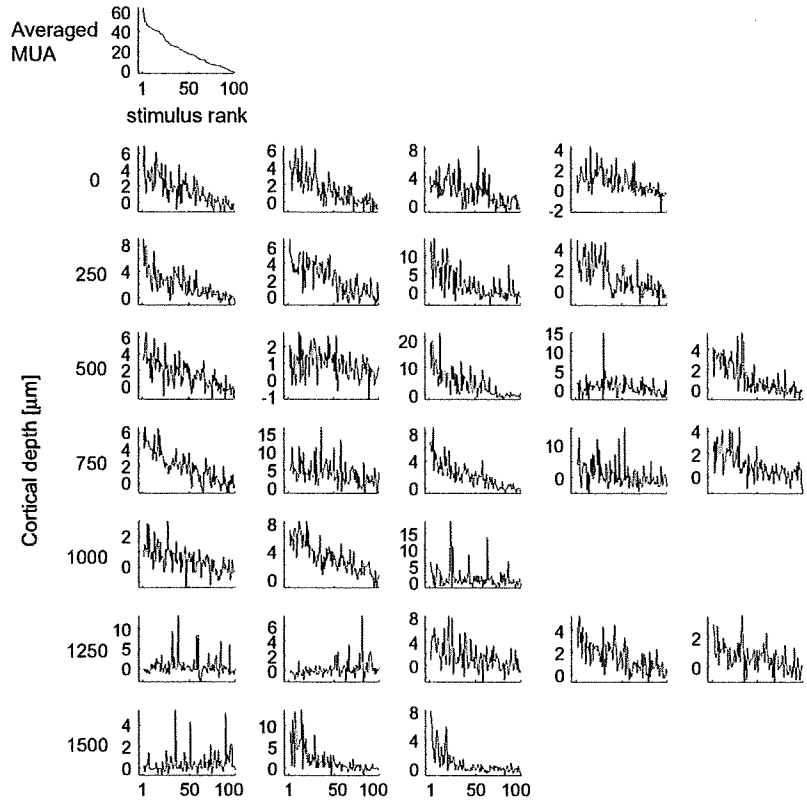

Figure 17. Tuning curves of the individual cells in a representative spot and the tuning curve of averaged MUs of the spot. The graph at the left upper corner represents the tuning curve of averaged MUs and the rests represent tuning curves of single cells at different depths. Depth of cells in each row is indicated at the left. Horizontal axes are rank ordered according to the magnitude of evoked responses of averaged MUs to the 100 object stimuli in descending order. Vertical axes represent mean firing rate (spikes/s).

examined for individual cells in the spots, correlation coefficients calculated for 100 object images may be biased to 20 object images used for intrinsic signal imaging. We calculated 2 values for correlation coefficients: one for 100 object images and the other for 80 object images where images used for intrinsic signal imaging were excluded. We did not find any qualitative difference in these 2 values as mentioned in the Results. Second, we considered a possibility that only part of IT cortex is organized in columns where neurons having similar response property are densely clustered, and intrinsic signal imaging extracted such columnar regions as activity spots. In hemisphere H2, where we did not conduct intrinsic signal imaging, the general tendencies of similarity among the cells were the same as those observed in the hemispheres with intrinsic signal imaging. In particular, the relationship between Figures 15(D) and (E) was consistent with the relationship between Figures 7(*Aa,Ba*) and (*Ab,Bb*), supporting the idea of columnar organization as a general functional structure in area TE. However, the values for correlation coefficients are lower than those values obtained from cells within the spots identified by intrinsic signal imaging. Specifically, similarity in object selectivity of MU pairs was almost the same as that of single-cell pairs for randomly chosen sites (Fig. 16*B*). There are 2 possible explanations for this difference caused by whether neuronal recordings were made from the activity spots or not. One explanation is that the recording sites were accidentally located at the border of 2 columns with different response properties. Previously, with intrinsic signal imaging, we found that activity spots elicited by similar but different stimuli tend to partially overlap each other (Wang et al. 1996, 1998), and thus, the columnar organization in area TE would be like orientation columns in area V1 where response properties gradually change along the cortical surface (Tanaka 1996). Thus, it is not likely that the recording sites were located at the border of distinct columns. Another possibility is that a part of the cortex is organized in columns, but response properties of the neurons within the columns were not as similar as the activity spots identified by intrinsic signal imaging. In intrinsic signal imaging, the optical signal is proportional to the number of cells that responded to the presented stimulus, and activity spots were the sites that revealed local maxima of the optical signals (Tsunoda et al. 2001). Because of the small size of the optical signal, the activity spots could be biased to the regions that contained a large number of neurons that shared the same response properties. Thus, the cortex may be organized in a region where neurons with similar response properties were densely clustered (highly columnar region) and a region where neurons with similar response properties were sparsely clustered (less columnar region). The result showing the difference between optically identified spots and randomly chosen sites (Fig. 16) is consistent with this idea. Taking into account that IT cortex is highly plastic even in adults and that this plasticity is essential for the memory function of this area, the less columnar region could be considered as a reserved area for future use. The idea of mosaic organization of IT cortex with highly columnar and less columnar regions is interesting, but still speculative because

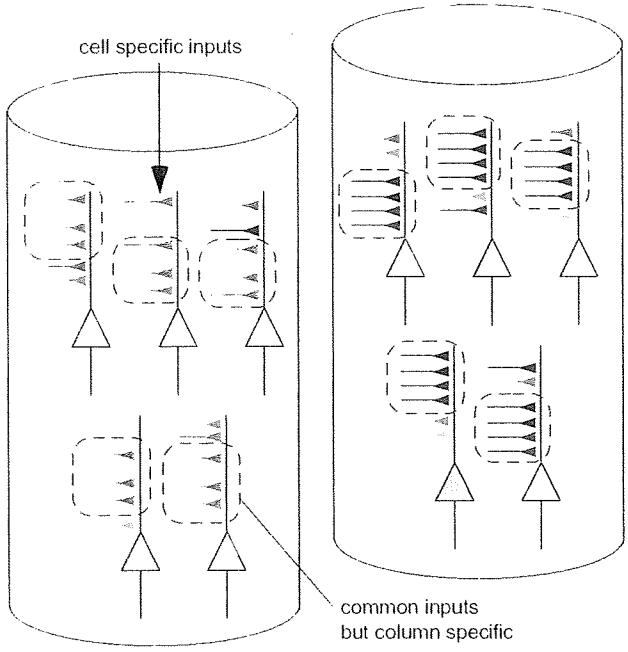

Figure 18. Schematic drawing of cell-specific inputs and inputs common among cells within a spot. Two columns are represented. The synaptic inputs demarcated by broken lines represent common inputs. These inputs are different from column to column. In this figure, the differences in common inputs for the 2 columns are indicated by the color of the inputs (left column, gray and right column, pink). Other inputs represent cell-specific synaptic inputs. We consider that these differences in synaptic inputs generate common and cell-specific response properties.

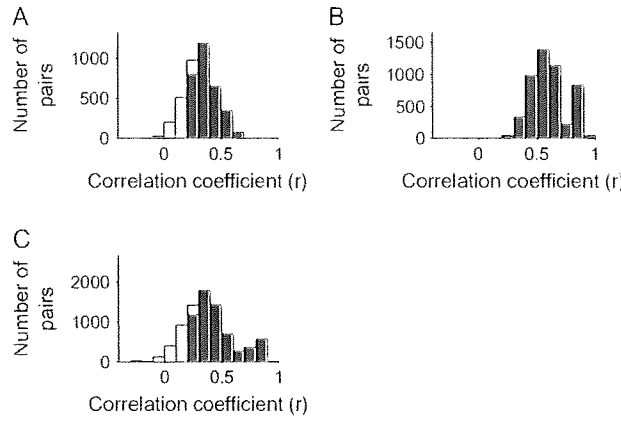

Figure 19. Demonstration showing increase of similarity in object selectivity by averaging activities of single cells. In each hemisphere, isolated cells were divided into 2 groups with equal number, and each group is averaged. A correlation coefficient was calculated between the evoked responses to 80 object images of these 2 averaged groups. Isolated cells were divided into 2 groups in 1000 different combinations, and resulting correlation coefficients were plotted in frequency distribution against the values of correlation coefficients. (*A*, *B*, *C*) were the frequency distribution obtained from hemispheres H1, H3, and H2, respectively. The mean and SD of the correlation coefficients were 0.35 − 0.11, 0.59 − 0.16, and 0.41 − 0.20 for H1, H3, and H2, respectively. The column in red represents the pairs with significant correlation ($P < 0.05$, $r = 0.22$).

evidence provided by comparison between hemispheres with and without intrinsic signal imaging is indirect.

Although in an idealized model, a column with neurons of similar response properties extends from the cortical surface down to the white matter, this is not necessarily the case in real brains. In ocular dominance columns in area V1, for example, neurons exclusively responding to the visual stimulus given to one eye are found in layer 4 but not in superficial and deeper layers (Hubel and Wiesel 1972). Similarly in area TE, we found that neurons with stimulus selectivity significantly correlated with averaged MUs were more frequently found in layers above layer 4 (Fig. 6*Ac*,*Bc*). Thus, although there is a columnar spatial organization in area TE, there was some bias in superficial layers, including layer 4. In the case of area V1, critical response properties such as ocular dominance and orientation preference are primarily determined by the geniculate inputs to the area. Taking this into account, the bias to upper layers may reflect specificity of inputs to area TE from area TEO. In fact, it has been shown that area TEO projects not only to layer 4 but also to layers above layer 4 (Saleem et al. 1993).

The systematic analysis of columnar organizations in area TE was first conducted by Fujita et al. They obtained evidence suggesting columnar organization in area TE by using a stimulus simplification procedure to find the simplest visual feature for each cell (Fujita et al. 1992). It is likely that their stimulus simplification procedure led them to reach the common property across cells within a columnar region. Their stimulus simplification procedure (Tanaka et al. 1991), however, was not entirely objective, and thus, we cannot exclude the possibility that their analysis was biased. The importance of the present study is that we showed the existence of one or potentially a few numbers of common properties across the cells in a columnar region with respect to object selectivity without such procedural bias.

Funding

Brain Science Institute, RIKEN. Funding to pay the Open Access publication charges for this article was provided by Brain Science Institute, RIKEN.

Notes

We thank Dr Kazushige Tsunoda for assistance with the surgical procedures and particularly for the procedure to expose the cortical surface. We also thank Ms Kei Hagiya for assistance during surgical procedures, Mr Hideyuki Watanabe for helping us for making the analysis software, and Ms Toshiko Ikari and Mr Mark Lescroart for comments on the manuscripts. *Conflict of Interest*: None declared.

Address correspondence to Manabu Tanifuji, Laboratory for Integrative Neural Systems, RIKEN Brain Science Institute, 2-1 Hirosawa, Wako-shi, Saitama 351-0198, Japan. Email: tanifuji@riken.jp.

Appendix

In the present paper, we regarded the activities of an MU as the sum of activities of single cells. Although activities of single cells are indeed involved in an MUA, increase of object similarity in MUs and averaged MUs may be due to potential differences in single-cell activities and MUAs other than the number of cells that are involved. Here, we arbitrarily divided isolated single cells recorded within a spot into 2 groups, A and B, and examined whether the value of the correlation coefficient between evoked responses of averaged activities of group A and those of group B was higher than the values obtained for isolated neuron pairs. To avoid the 2 groups accidentally giving a high value of the correlation coefficient, we performed a permutation analysis where isolated cells were divided into groups A and B in various ways, correlation coefficients were calculated for individual grouping, and mean values ± SD of correlation coefficients were calculated (Fig. 19). The resulting values of correlation coefficients for H1, H3, and H2 were 0.32 ± 0.14, 0.60 ± 0.15, and 0.39 ± 0.21, respectively. These values were

higher than the mean value of correlation coefficients for isolated pairs of H1, H3, and H2, which were 0.11 ± 0.21, 0.15 ± 0.22, and 0.10 ± 0.24, respectively. These values were even larger than the mean value of MU pairs, which were 0.23 ± 0.20, 0.28 ± 0.26, and 0.10 ± 0.16 for H1, H2, and H3, respectively. These results support the idea that in MUs and in averaged MUs, cell-to-cell variability in object selectivity was removed and common properties were extracted.

References

Albright TD, Desimone R, Gross CG (1984) Columnar organization of directionally selective cells in visual area MT of the macaque. J Neurophysiol 51:16–31.

Arieli A, Grinvald A, Slovin H (2002) Dural substitute for long-term imaging of cortical activity in behaving monkeys and its clinical implications. J Neurosci Methods 114:119–133.

Baker C, Knouf N, Wald L, Fischl B, Kwang K, Benner T, Kanwisher N (2004) Functional selectivity of human extrastriate visual cortex at high resolution. J Vis 4:88–88.

Cheng K, Waggoner RA, Tanaka K (2001) Human ocular dominance columns as revealed by high-field functional magnetic resonance imaging. Neuron 32:359–374.

Desimone R, Albright TD, Gross CG, Bruce C (1984) Stimulus-selective properties of inferior temporal neurons in the macaque. J Neurosci 4:2051–2062.

Fujita I, Tanaka K, Ito M, Cheng K (1992) Columns for visual features of objects in monkey inferotemporal cortex. Nature 360:343–346.

Fukuda M, Moon CH, Wang P, Kim SG (2006) Mapping iso-orientation columns by contrast agent-enhanced functional magnetic resonance imaging: reproducibility, specificity, and evaluation by optical imaging of intrinsic signal. J Neurosci 26:11821–11832.

Gochin PM, Miller EK, Gross CG, Gerstein GL (1991) Functional interactions among neurons in inferior temporal cortex of the awake macaque. Exp Brain Res 84:505–516.

Gross CG, Rocha-Miranda CE, Bender DB (1972) Visual properties of neurons in inferotemporal cortex of the macaque. J Neurophysiol 35:96–111.

Hubel DH, Wiesel TN (1962) Receptive fields, binocular interaction and functional architecture in the cat's visual cortex. J Physiol 160:106–154.

Hubel DH, Wiesel TN (1972) Laminar and columnar distribution of geniculo-cortical fibers in the macaque monkey. J Comp Neurol 146:421–450.

Kobatake E, Tanaka K (1994) Neuronal selectivities to complex object features in the ventral visual pathway of the macaque cerebral cortex. J Neurophysiol 71:856–867.

Kreiman G, Hung CP, Kraskov A, Quiroga RQ, Poggio T, DiCarlo JJ (2006) Object selectivity of local field potentials and spikes in the macaque inferior temporal cortex. Neuron 49:433–445.

Malonek D, Tootell RB, Grinvald A (1994) Optical imaging reveals the functional architecture of neurons processing shape and motion in owl monkey area MT. Proc R Soc Lond B Biol Sci 258:109–119.

Mountcastle VB (1957) Modality and topographic properties of single neurons of cat's somatic sensory cortex. J Neurophysiol 20:408–434.

Perrett DI, Smith PA, Potter DD, Mistlin AJ, Head AS, Milner AD, Jeeves MA (1984) Neurones responsive to faces in the temporal cortex: studies of functional organization, sensitivity to identity and relation to perception. Hum Neurobiol 3:197–208.

Przybyszewski AW, Sato T, Fukuda M (2008) Optical filtering removes non-homogenous illumination artifacts in optical imaging. J Neurosci Methods 168:140–145.

Rolls ET, Tovee MJ (1995) Sparseness of the neuronal representation of stimuli in the primate temporal visual cortex. J Neurophysiol 73:713–726.

Saleem KS, Tanaka K, Rockland KS (1993) Specific and columnar projection from area TEO to TE in the macaque inferotemporal cortex. Cereb Cortex 3:454–464.

Tamura H, Kaneko H, Fujita I (2005) Quantitative analysis of functional clustering of neurons in the macaque inferior temporal cortex. Neurosci Res 52:311–322.

Tanaka K (1996) Inferotemporal cortex and object vision. Annu Rev Neurosci 19:109–139.

Tanaka K, Saito H, Fukada Y, Moriya M (1991) Coding visual images of objects in the inferotemporal cortex of the macaque monkey. J Neurophysiol 66:170–189.

Tsao DY, Freiwald WA, Tootell RB, Livingstone MS (2006) A cortical region consisting entirely of face-selective cells. Science 311:670–674.

Tsunoda K, Yamane Y, Nishizaki M, Tanifuji M (2001) Complex objects are represented in macaque inferotemporal cortex by the combination of feature columns. Nat Neurosci 4:832–838.

Wang G, Tanaka K, Tanifuji M (1996) Optical imaging of functional organization in the monkey inferotemporal cortex. Science 272:1665–1668.

Wang G, Tanifuji M, Tanaka K (1998) Functional architecture in monkey inferotemporal cortex revealed by in vivo optical imaging. Neurosci Res 32:33–46.

Yamane Y, Tsunoda K, Matsumoto M, Phillips AN, Tanifuji M (2006) Representation of the spatial relationship among object parts by neurons in macaque inferotemporal cortex. J Neurophysiol 96:3147–3156.

Jpn J Ophthalmol 2009;53:449–451
DOI 10.1007/s10384-009-0708-1

CLINICAL INVESTIGATION

Optical Coherence Tomographic Evaluation of the Outer Retinal Architecture in Oguchi Disease

Kisaburo Yamada, Yuka Motomura, Celso S. Matsumoto, Kei Shinoda, and Kazuo Nakatsuka

Department of Ophthalmology, Oita University Faculty of Medicine, Oita, Japan

Abstract

Background: To report the changes in the optical coherence tomography (OCT) images of the outer retinal layers after prolonged dark adaptation in a patient with Oguchi disease.

Case: A 75-year-old woman showed the typical golden-yellow fundus reflex of Oguchi disease, and the coloration returned to normal after prolonged dark adaptation. Fourier domain OCT (FD-OCT) was performed on the patient's left eye before and after prolonged dark adaptation.

Observations: Before dark adaptation, the FD-OCT images at the fovea had three identifiable reflection bands, namely, the external limiting membrane (ELM), the border between the photoreceptor inner and outer segments (IS/OS line), and the retinal pigment epithelium (RPE)/Bruch band. The paramacular area had only the ELM and RPE/Bruch bands. After 4 h of dark adaptation, the IS/OS line was also detected in the paramacular area.

Conclusions: The absence of the IS/OS line in the extramacular regions in the partly dark adapted condition was most likely due to a defect in the rod photoreceptors of this area. The emergence of the IS/OS line after prolonged dark adaptation suggests that microarchitectural changes occur in the photoreceptors and that the changes may be correlated with the improvement of rod function. **Jpn J Ophthalmol** 2009;53:449–451 © Japanese Ophthalmological Society 2009

Keywords: inner segment/outer segment line, Oguchi disease, optical coherence tomography, photoreceptors

Introduction

Recent improvements in the resolution of optical coherence tomography (OCT) instruments have greatly enhanced the ability of investigators to evaluate the fine structure of the retina. Quantitative measurements of retinal images obtained by these instruments have shown that photoreceptors can be altered in several macular diseases.[1] These measurements are made on four highly reflective lines in the OCT images. These lines have been identified as the external limiting membrane (ELM), the border between the photoreceptor inner and outer segments (IS/OS line), the so-called Verhoeff's membrane or intermediate line (IML), where the tips of the cone photoreceptor outer segments are enveloped by microvilli, and the retinal pigment epithelium (RPE)/Bruch band.[2]

We present the OCT-determined morphological appearance of photoreceptors in the eye of a patient with Oguchi disease before and after 4 h of dark adaptation. The time of appearance of the morphological changes coincided with the return to normal of fundus coloration.

Case Report

Ophthalmoscopic examination of a 75-year-old woman showed that her fundus had the golden-yellow reflex typical of eyes with Oguchi disease (Fig. 1). Dark adaptometry showed that her dark adaptation was delayed, as is typical of patients with Oguchi disease. The full-field bright-flash

Received: March 31, 2009 / Accepted: April 6, 2009
Correspondence and reprint requests to: Kei Shinoda, Department of Ophthalmology, Oita University Faculty of Medicine, Hasama-machi, Yufu, Oita 879-5593, Japan
e-mail: shinodak@med.oita-u.ac.jp

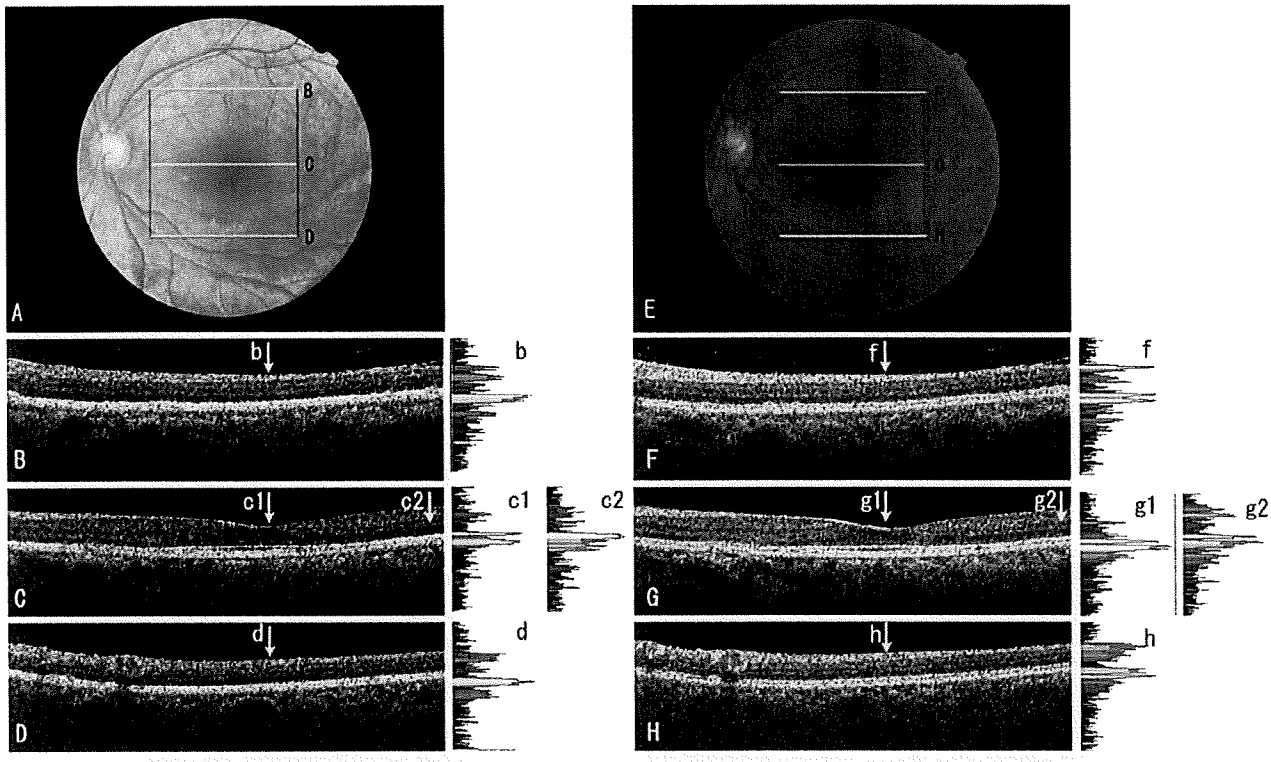

Figure 1A–H. Fundus photographs and Fourier domain optical coherence tomographic (FD-OCT) images of the eyes of a patient with Oguchi disease before and 3 h after dark adaptation. **A** Fundus photograph of the left eye before dark adaptation showing typical golden-yellow reflex. The yellow bars indicate scanning lines for the cross-sectional FD-OCT images shown in **B–D**. **B** Horizontal cross-sectional OCT image 3 mm superior to the fovea. The graph to the right of the image shows the reflective intensity at each vertical point in the scan 3 mm superior to the fovea (location *b*). Only a single highly reflective thick band is seen. **C** Horizontal cross-sectional OCT image of the fovea. The graph to the right of the image shows the reflective intensity at each vertical point through the fovea (location *c1*) and a location approximately 2.5 mm temporal to the fovea (location *c2*). At the fovea, the retinal outer layer is made up of two layers: the boundary between the inner and outer segments (IS/OS line) and the retinal pigment epithelium (RPE)/Bruch band. In the extrafoveal area, only a single highly reflective thick band is seen; the IS/OS line cannot be seen. **D** Horizontal cross-sectional OCT image 3 mm inferior to the fovea. The graph to the right of the image shows the reflective intensity at each vertical point through the image at location *d*. Only a single highly reflective thick band is seen. **E** Fundus photograph and scanning area of the FD-OCT of the patient after 3 h of dark adaptation showing normal coloration of the fundus reflex. The yellow lines indicate scanning lines for the cross-sectional images shown in **F–H**. **F** Horizontal cross-sectional OCT image 3 mm superior to the fovea. The graph to the right of the image shows the reflective intensity at each vertical point through the image at location *f*. this image is at the same location as that shown in **B**. The intensity of the retina is made up of two highly reflective bands: the IS/OS line and the RPE/Bruch band. **G** Horizontal cross-sectional OCT image through the fovea. The image was obtained approximately 2.5 mm temporal to the fovea, like that shown in **C**. The graph to the right of the image shows the reflective intensity at each vertical point through the image at locations *g1* and *g2*. At both locations, the retinal outer layer comprises two sublayers: most likely the IS/OS line and RPE/Bruch band. **H** Horizontal cross-sectional OCT image 3 mm inferior to the fovea. The graph to the right of the image shows the reflective intensity at each vertical point through the image at location *h*. This scan is at the same location as that shown in **D**. The retina is made up of two highly reflective bands: most likely the IS/OS line and RPE/Bruch band.

electroretinograms (ERGs) had a negative shape (b/a ratio < 1), which is also typical of Oguchi disease. Both the scotopic and photopic ERGs were reduced.

After 4 h of dark adaptation, the color of the fundus appeared normal (the so-called Mizuo-Nakamura phenomenon), and the subjective visual threshold improved, although it did not reach normal levels. All of these findings are compatible with Oguchi disease.

OCT images were obtained with the Fourier domain OCT-1000 (FD-OCT; Topcon, Tokyo, Japan). The area scanned was 6.0 mm × 6.0 mm at a depth of 4.0 mm. A three-dimensional data set was acquired using the default setting of 512 × 128 raster pixels, which represented a horizontal pixel resolution of 11.7 μm and a vertical pixel resolution of 46.9 μm.

Three easily identifiable layers, namely, the ELM, IS/OS line, and RPE/Bruch band, were detected in the FD-OCT images of the fovea (Fig. 1) in the partly dark-adapted state. However, only two distinct lines were discernible in the paramacular area, where the density of cone photoreceptors is low. The innermost line was identified as the ELM, and the second line was a thickened, highly reflective RPE/Bruch band.

After 4 h of dark adaptation, the FD-OCT images of the fovea did not change, but the extramacular area showed another highly reflective band just vitread of the RPE/Bruch

band. This new band corresponded to the IS/OS line, because it was continuous with the IS/OS line of the fovea. The appearance of this band coincided with the normalization of the fundus color.

Discussion

The absence of the IS/OS line in the extrafoveal area in the partly dark-adapted state in our patient with Oguchi disease is similar to that reported in several macular diseases.[1] We suggest that the IS/OS line may have been integrated into the RPE/Bruch band in this state of adaptation. The absence of the IS/OS line coincided with the time when the visual threshold was high and the rods most likely nonfunctional, as evidenced by the elevated visual threshold. After prolonged dark adaptation, the recovery of the visual threshold and normal coloration of the fundus were correlated with the appearance of the IS/OS line. In our case, the correlation of the presence of the IS/OS line with the other two conditions strongly suggests a causative relationship.

Although the presence of the IS/OS line was correlated with the functional state of the rods, the IS/OS line was clearly observed at the foveal area, where the rods are absent or very few in number. This suggests that the presence of the IS/OS line may not depend only on the presence of normally functioning rods. In healthy eyes, the IS/OS line can also be detected in the extrafoveal area, where the density of rods is high and that of cones is low. The correlation of the return of the IS/OS line and the decrease of the visual threshold to near normal levels in our patient indicated that the physiological condition of the rods must have been normal for the IS/OS line to be visible. Thus, we suggest that the absence of the IS/OS line in the extrafoveal area may be the morphological manifestation of the functional alteration of the rods that was detected by the elevated visual threshold. If so, this finding indicates that the functional state of the rods can be assessed by the presence of the IS/OS line in FD-OCT images.

After examining the fundus of a patient with Oguchi disease with a helium-neon laser (633 nm) scanning laser ophthalmoscope (SLO), Usui et al.[3] reported the presence of diffuse, fine, white particles, which were not detected in healthy participants. The abnormal particles disappeared after 4 h of dark adaptation and reappeared gradually during 30 min of light adaptation, coinciding with the appearance of the golden metallic reflex. They suggested that the particles were located in the outer retina or retinal pigment epithelium, and could be the cause of the abnormal fundus appearance in Oguchi disease.

The pathologic site of the abnormal ERGs in Oguchi disease was suggested by Miyake et al.[4] to be between the photoreceptors and the bipolar cells of the phototransduction pathway. However, the site and mechanism of the characteristic fundus coloration and its changes after dark adaptation have still not been determined. The coincidental changes in the FD-OCT images of the outer retina and the changes in the coloration of the fundus suggest that the region around the photoreceptor outer segments is the site of the abnormal coloration. Further investigations with simultaneous observations of the fundus by SLO and OCT may help disclose the relationship between the particles and the structural and functional changes of the rods.

Interesting observations have been recently made by functional optical imaging, in particular, by functional OCT.[5] This new technique, called optophysiology, is important because, as our case clearly illustrates, morphological changes of the photoreceptors obtained by FD-OCT are correlated with the functional state of the photoreceptors. However, the visibility of the IS/OS line depends on several factors, such as resolution of the OCT, opacity of the media, and probably the pathology. In addition, the integrity of the IS/OS line can be altered by inflammation, edema, circulatory disturbances, and mechanical damage. Thus, many factors can affect the acquisition of OCT images necessary to perform a detailed analysis of the physiology of the retina.

Acknowledgments. Support for this study was provided by Researches on Sensory and Communicative Disorders from the Ministry of Health, Labour and Welfare, Japan, and from the Ministry of Education, Culture, Sports, Science and Technology, Japan.

References

1. Matsumoto H, Kishi S, Otani T, Sato T. Elongation of photoreceptor outer segments in central serous chorioretinopathy. Am J Ophthalmol 2008;145:162–168.
2. Zawadzki RJ, Choi SS, Jones SM, Oliver SS, Werner JS. Adaptive optics-optical coherence tomography: optimizing visualization of microscopic retinal structures in three dimensions. J Opt Soc Am A Opt Image Sci Vis 2007;24:1373–1383.
3. Usui T, Ichibe M, Ueki S, et al. Mizuo phenomenon observed by scanning laser ophthalmoscopy in a patient with Oguchi disease. Am J Ophthalmol 2000;130:359–361.
4. Miyake Y, Horiguchi M, Suzuki S, Kondo M, Tanikawa A. Electrophysiological findings in patients with Oguchi's disease. Jpn J Ophthalmol 1996;40:511–519.
5. Bizheva K, Pflug R, Hermann B, et al. Optophysiology: depth-resolved probing of retinal physiology with functional ultrahigh-resolution optical coherence tomography. Proc Natl Acad Sci U S A 2006;103:5066–5071.

Original Paper

Ophthalmologica

Ophthalmologica 325
DOI: 10.1159/000XXXXX

Received: December 20, 2007
Accepted after revision: March 13, 2008
Published online: ■■■

Photopic Negative Response Reflects Severity of Ocular Circulatory Damage after Central Retinal Artery Occlusion

Celso S. Matsumoto Kei Shinoda Kisaburo Yamada Kazuo Nakatsuka

Department of Brain and Neuroscience, Ophthalmology, Oita University, Oita, Japan

Key Words
Photopic electroretinogram · Photopic negative response · Central retinal artery occlusion · Fluorescein angiography

Abstract
Purpose: To determine the relationship of the photopic negative response (PhNR) of the photopic electroretinogram (ERG) with the degree of circulatory disturbances in eyes following central retinal artery occlusion (CRAO). ***Methods:*** The circulatory disturbance was graded as mild (group 1) when the arm-to-retina transmission time was <30 s, moderate (group 2) when the time was >30 s and severe (group 3) when concurrent choroidal circulatory damage was found. For statistical analysis, groups 1, 2 and 3 were scored as 1, 2 and 3, respectively. Photopic ERGs were elicited by either short-flash (SF) or long-flash (LF) stimuli. ***Results:*** Both the SF and LF PhNR were significantly reduced in groups 2 and 3. The PhNR amplitude was negatively correlated with the severity of the ocular circulatory disturbances ($p = 0.0498$, $\rho = -0.507$ for SF PhNR; $p = 0.0050$, $\rho = -0.750$ for LF PhNR). ***Conclusion:*** The amplitude of the PhNR became more reduced as the severity of the circulatory disturbances increased in eyes with CRAO.

Introduction

A central retinal artery occlusion (CRAO) is a devastating condition requiring immediate treatment because it leads to a sudden, painless and catastrophic visual loss over several seconds [1]. The retinal damage is progressive and often irreversible [2–4]. A decrease in the b-wave with a relatively well-preserved a-wave, leading to a negative type electroretinogram (ERG) [5, 6], is a well-known characteristic finding of the mixed rod-cone ERG. The mixed rod-cone ERG mainly reflects the neural activity of the neurons in the outer and inner retina but not that of the retinal ganglion cells (RGCs), which explains why the ERG findings are often inconsistent with the visual fields and visual acuities, e.g. eyes with extremely constricted visual fields and poor visual acuity can have well-preserved ERGs [7].

The RGCs are more vulnerable to ischemia and suffer irreversible damage soon after an occlusion, which is supported by histopathologic findings showing apoptotic changes in this layer [8]. The photopic negative response (PhNR) of the photopic ERG which originates from the neural activity of the RGCs has been used to assess the function of RGCs in experimental animals [9, 10] and in

KARGER
Fax +41 61 306 12 34
E-Mail karger@karger.ch
www.karger.com

0030–3755/09/0000–0000$26.00/0

Accessible online at:
www.karger.com/oph

Kei Shinoda, MD
Department of Brain and Neuroscience, Division of Sensory and Locomotive Science
Ophthalmology, Oita University Faculty of Medicine
Hasama-machi, Yufu-shi, Oita 879-5593 (Japan)
Tel. +81 975 86 5904 Fax +81 975 49 6043 E-Mail shinodak@med.oita-u.ac.jp

Table 1. Demographics of the patients with CRAO

Case	Age years	Gender	Affected eye	Group	First visit day	Visual acuity at first visit	Visual acuity at 1 month	Visual acuity at last visit
1	72	F	L	1	3	0.2	0.2	0.2
2	68	F	R	1	0	HM	0.02	0.02
3	81	F	R	1	2	0.06	0.1	0.1
4	73	F	R	1	1	HM	0.1	0.1
5	59	M	L	1	0	SL(+)	0.1	0.15
6	71	M	L	2	0	0.04	0.1	0.1
7	66	M	R	2	0	SL(−)	HM	CF
8[1]	79	M	R	2	10	HM	HM	HM
9	44	F	R	2	0	SL(−)	SL(+)	SL(+)
10	80	F	L	2	0	HM	0.01	0.01
11	61	M	L	2	0	HM	HM	HM
12	66	M	R	2	1	SL(−)	SL(−)	SL(−)
13	74	F	R	2	0	SL(−)	SL(+)	HM
14	40	M	R	3	0	SL(−)	SL(−)	SL(−)
15	74	F	R	3	0	0.02	SL(+)	SL(−)
16	74	M	L	3	14	HM	HM	HM

L = Left eye; R = right eye; HM = hand motion; SL = light sense. Group 1: arm-to-retina time <30 s; group 2: arm-to-retina time ≥30 s in fluorescein angiography; group 3: CRAO with choroidal circulation disturbance; 'first visit' day 0 = patient visited clinic within 24 h after onset.

[1] All patients developed unilateral CRAO and the healthy fellow eye served as control except in case 8 who developed branch retinal vein occlusion in the left eye.

humans with retinal and optic nerve pathology [10–15]. The findings of these experiments prompted us to investigate the relationship of the PhNR of the photopic ERGs with the degree of circulatory disturbances in eyes with a CRAO. In addition, the relation between the PhNR and the final visual acuity was investigated.

In the earlier studies [10–13], the PhNR analysis was made in the recordings of photopic ERG that was elicited by a short stimulus (<6 ms), and the amplitude of the PhNR might be affected by the i-wave [16–18]. The photopic ERG using long-duration (150 ms) stimuli can minimize the influence of the i-wave, which is thought to be associated with the off component [10, 18, 19] of the photopic ERG. Therefore, another focus of this study was to analyze the PhNR elicited by short- and long-duration stimuli.

Patients and Methods

The medical records of 16 eyes of 16 consecutive patients with CRAO which was diagnosed at Oita University Hospital from 2003 to 2007 were examined. The procedure used in this study conformed to the tenets of the Declaration of Helsinki. Informed consent was obtained from all patients before the ERG recordings.

A complete ophthalmologic examination was performed on each patient. We classified the degree of ocular circulation disturbance into 3 groups according to fluorescein-angiographic findings. In group 1 (mild), the arm-to-retina transmission time in fluorescein angiography was <30 s; in group 2 (moderate), the fluorescein-angiographic arm-to-retina transmission time was ≥30 s, and in group 3 (severe), a concurrent choroidal perfusion disturbance was detected by fluorescein angiography and indocyanine green choroidal angiography. For statistical analysis, groups 1, 2 and 3 were scored as 1, 2 and 3, respectively.

Patients with other retinal diseases were excluded. All emergency treatment procedures (ocular massage, lowering of intraocular pressure, thrombolytic agent administration) were performed before or at the time of the ERG recordings. ERGs were recorded from all 16 eyes with a CRAO and the fellow eyes. Fifteen of the 16 fellow eyes were normal and served as controls. One eye developed a branch retinal vein occlusion and was not analyzed. The clinical findings of the patients with a CRAO are presented, in table 1.

The intraocular pressure (IOP) was measured before each ERG recording by applanation tonometry. Any patient with an intraocular pressure >19 mm Hg was excluded because if elevated, it can alter the ERG [20, 21].

Electroretinography

The photopic ERGs were recorded from all eyes. The patient's pupils were fully dilated with 0.5% tropicamide and 0.5% phenylephrine hydrochloride eyedrops. The ERG responses were re-

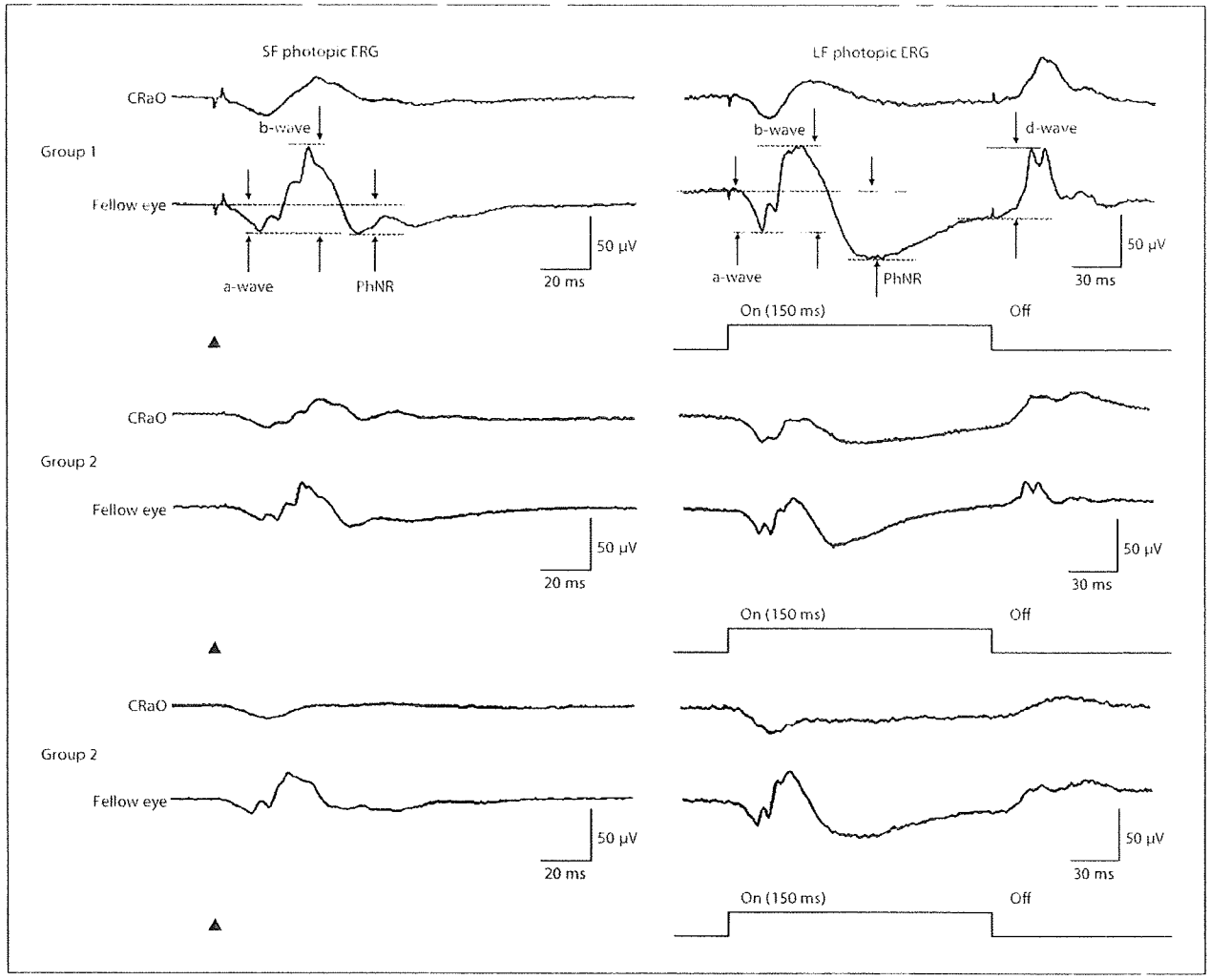

Fig. 1. Photopic ERGs elicited by short-flash (SF, 1 ms) and long-flash (LF, 150 ms) stimuli in eyes with a CRAO and the healthy fellow eyes. Triangles indicate short-duration stimuli.

corded from the anesthetized cornea with a corneal bipolar electrode (Z7285, Mayo Corp., Japan). A 10-min period of light adaptation preceded the photopic recordings. Responses were differentially amplified with an AC bioamplifier (Neuropack Σ, Nihon Kohden, Japan) and filtered by a bandpass filter from 0.1 and 1,000 Hz to yield the a- and b-waves and the PhNR. The ERGs were digitalized with a 12-bit A/D board (AD 32/10HD, Contec, Japan), and averaged online and offline if necessary, using a customized software (Multi Analyser EP, MTS, Japan).

The stimulus flashes were delivered in a customized Ganzfeld color dome stimulator 30 cm in diameter. The photopic ERGs were elicited with flashes of white light from a high-current type LED stimulator. ERGs were elicited by both photopic short duration (3 ms, 1,000 cd/m^2, 0.9 Hz) on a light-adapting field of 25 cd/m^2 (white background), and long-duration stimuli (150 ms, 300 cd/m^2, 0.9 Hz) of white light pulses on a light-adapting field of 40 cd/m^2 (white background). Four ERGs were averaged.

Representative photopic ERGs elicited by short- and long-duration stimuli are shown in figure 1. The amplitudes and implicit times of the a- and b-waves and the PhNRs were measured as shown in figure 1. One-factor analysis of variance followed by Fisher's protected least significant difference post hoc test was performed to evaluate differences among the 4 groups, i.e., 3 groups of diseased eyes and a control group of healthy fellow eyes. A comparison of PhNR amplitude between eyes with relatively good visual acuity (VA $\geq$0.1) and eyes with poor acuity (VA <0.1) was made by t test. A p value <0.05 was considered statistically significant.

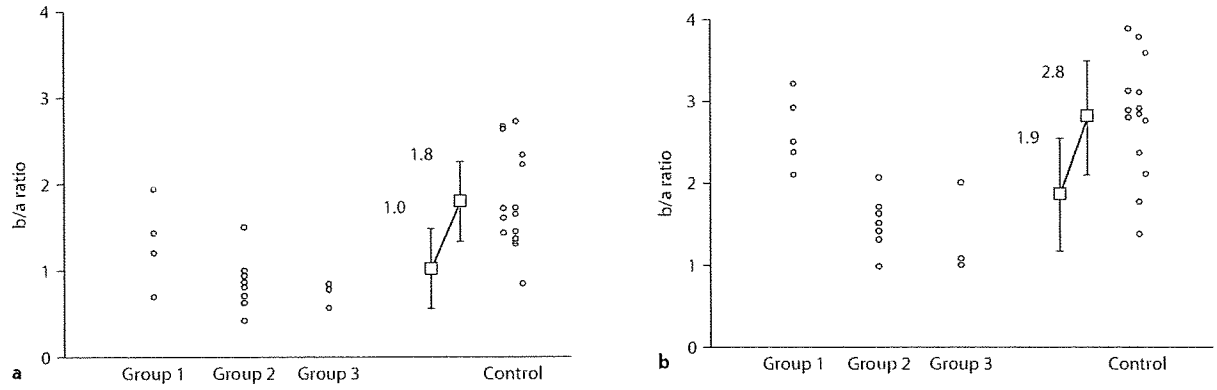

Fig. 2. The b-wave/a-wave ratio of the photopic ERG elicited by long- (**a**) and short-duration (**b**) stimuli. The average of the b/a ratio was smaller in CRAO eyes than in control eyes. ○ = Each individual b/a ratio; ⊐ = averaged b/a ratio (all CRAO groups vs. controls). **a** For the photopic ERGs elicited by long-duration stimuli, 11 (68.8%) of 16 eyes with a CRAO had a negative type pattern (b/a ratio <1.0). **b** For the photopic ERGs elicited by short-duration stimuli, only 1 (6.3%) of 16 eyes had a negative pattern.

Results

The demographics of the patients are shown in table 1. The patients were 8 men and 8 women whose ages ranged from 40 to 81 years (mean ± SD 67.6 ± 11.8). Of the 16 eyes, 5 were placed into group 1, 8 into group 2 and 3 into group 3.

At the initial visit, the VA ranged from no light perception to 0.2 with a median of hand motion vision. Only 1 eye in group 1 had a VA ≥0.1. At the last follow-up examination, the VA ranged from no light perception to 0.2 with a median of hand motion vision. However, 4 eyes had a VA ≥0.1.

The b-wave/a-wave ratios of the photopic ERG elicited by long- and short-duration stimuli are shown in figure 2. The average of the b/a ratio was low in eyes with a CRAO. Eleven (68.8%) of 16 eyes with a CRAO had a negative type, i.e., b/a ratio <1.0, for the long-duration photopic ERGs (long-flash (LF) photopic ERG), while only 1 (6.3%) of 16 eyes had the negative type (b/a ratio <1.0) for the short-duration photopic ERGs (short-flash (SF) photopic ERG).

A summary of the amplitudes of each component of the photopic ERGs elicited by long- and short-duration stimuli are shown in figures 3 and 4. The average a-wave amplitude in the eyes with a CRAO was only significantly smaller than that of the control eyes in group 3 (fig. 3). The average b-wave amplitude was significantly smaller than that of control eyes in groups 2 and 3 (fig. 3). The average d-wave amplitude was not significantly different from that in controls in all groups (fig. 4). The average amplitude of the LF PhNR was significantly smaller than that of control eyes in groups 2 and 3, but the amplitude of the SF PhNR was significantly smaller than that of the control eyes in all 3 groups (fig. 4). In addition, the amplitudes of the SF and LF PhNRs were negatively correlated with the severity of the ocular circulatory disturbances ($p = 0.0498$, $\rho = -0.507$ and $p = 0.0050$, $\rho = -0.750$, respectively), i.e., the amplitude decreased as the severity increased. The amplitudes of the b- and d-waves of the photopic ERGs elicited by long-duration stimuli were also negatively correlated with the severity of the ocular circulatory disturbances ($p = 0.0062$, $\rho = -2.739$ and $p = 0.0130$, $\rho = -2.483$ for b-wave and d-wave, respectively). The a-waves were also reduced, but they were not significantly correlated with the other 2 parameters.

The amplitudes of the PhNR elicited by short- and long-duration stimuli in eyes with a VA ≥0.1 and eyes with a VA <0.1 at 1 month and at the last visit (2–8 months) are shown in figure 5. The amplitude of the PhNRs elicited by long-duration stimuli were significantly larger ($p = 0.0168$) in eyes with a VA ≥0.1 than in eyes with a VA <0.1 both at 1 month and the last visit. The amplitude of the b-wave elicited by long- or short-duration stimuli was also significantly larger ($p = 0.0002$ and 0.0118, respectively) in eyes with a VA ≥0.1 than in eyes with a VA <0.1 both at 1 month and the last visit, whereas the a-wave and the d-wave were not significantly dif-

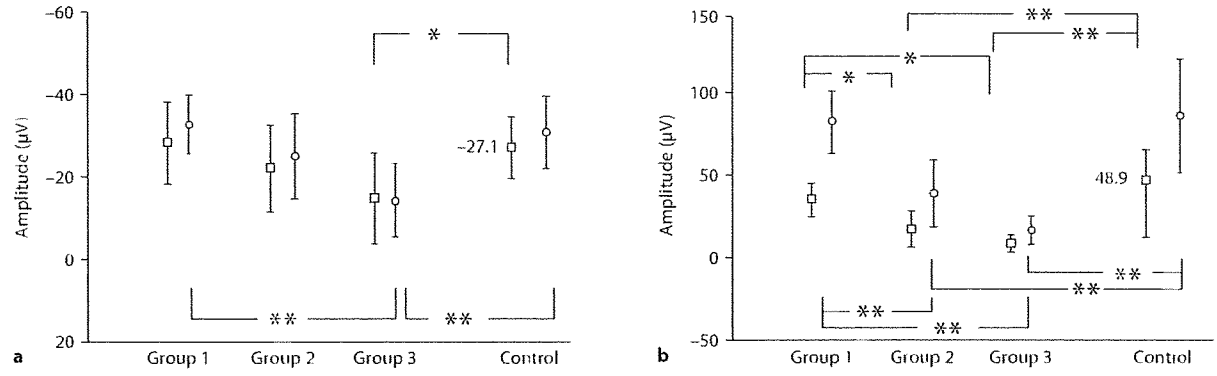

Fig. 3. Amplitudes of the a-waves (**a**) and b-waves (**b**) of the photopic ERGs elicited by long- and short-duration stimuli. □ = LF photopic ERG; ○ = SF photopic ERG; * $p < 0.05$, ** $p < 0.01$. **a** The average a-wave amplitude in the eyes with a CRAO was only significantly smaller than that of control eyes in group 3. The a-waves decreased as the severity increased, but the correlation was not statistically significant. **b** The averaged b-wave amplitude was significantly smaller than that of the control eyes in groups 2 and 3. Amplitudes of the b-wave of the photopic ERG recorded following long-duration stimuli are negatively correlated with the severity of the ocular circulatory disturbances ($p = 0.0062$, $\rho = -2.739$).

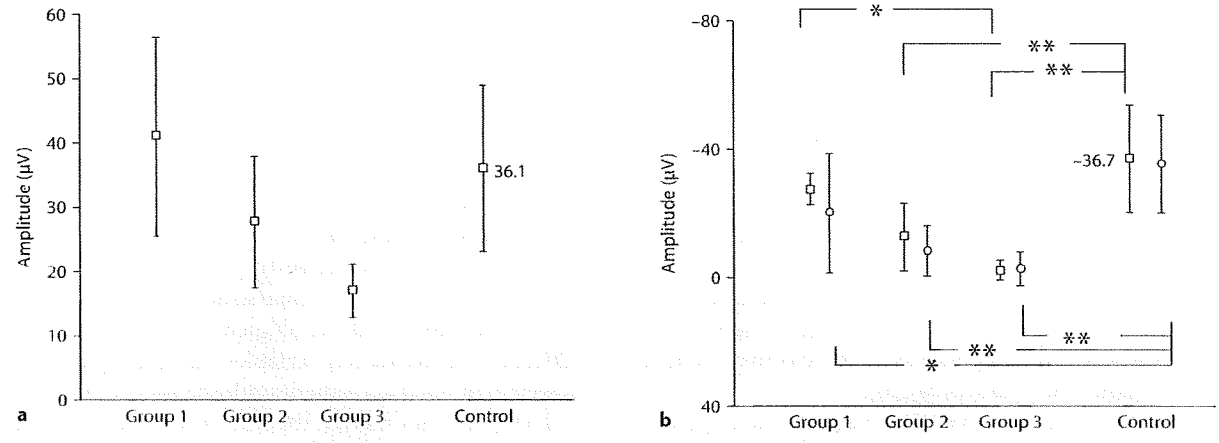

Fig. 4. Amplitude of the d-wave of PhNR in photopic ERG elicited by long-duration stimuli (**a**) and the amplitudes of PhNR in photopic ERG elicited by long- and short-duration stimuli (**b**). **a** The averaged d-wave amplitude was smaller compared to control eyes in groups 2 and 3, but significance was not reached. The d-wave amplitude of the photopic ERG recorded following long-duration stimuli was negatively correlated with the severity of the ocular circulatory disturbances ($p = 0.0130$, $\rho = -2.483$). **b** The averaged LF PhNR amplitude was significantly decreased compared to control eyes in groups 2 and 3, whereas the amplitude of the SF PhNR was significantly decreased compared to control eyes in all 3 groups. The amplitudes of the SF and LF PhNR were negatively correlated with the severity of the ocular circulatory disturbances ($p = 0.0498$, $\rho = -0.507$ and $p = 0.0050$, $\rho = -0.750$ for SF PhNR and LF PhNR, respectively). □ = LF photopic ERG; ○ = SF photopic ERG; * $p < 0.05$; ** $p < 0.01$.

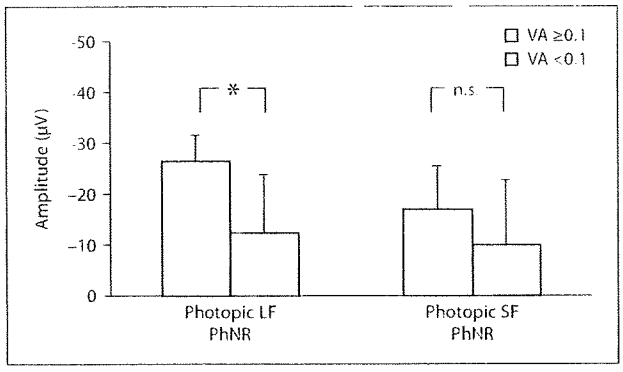

Fig. 5. Comparison of the amplitude of SF or LF PhNR between eyes of VA ≥0.1 (n = 5) and eyes of VA <0.1 (n = 11) at 1 month and at the last visit. The amplitude of the LF PhNR was significantly larger ($p = 0.0168$) in eyes with VA ≥0.1 compared to eyes with VA <0.1 both at 1 month and the last visit, suggesting that the LF PhNR had been better preserved in eyes which later attained relatively better VA in CRAO cases. * $p < 0.05$; n.s. = not significant.

ferent between eyes with a VA ≥0.1 and eyes with a VA <0.1. This would suggest that the LF PhNR and the b-wave were better preserved in eyes which later attained a relatively better VA in CRAO cases.

Discussion

In primate models of transient CRAO, irreversible retinal damage occurs after 100 min of ischemia [3, 4]. In humans, a recovery of visual function has been reported in cases more than 18 h after the onset of CRAO [22], suggesting that the retina can tolerate a transient obstruction of blood flow. However, very little information is available on how to evaluate the effects of the retinal ischemia and to predict the visual prognosis.

The ERGs of eyes with a CRAO are characterized by a reduced b-wave with a relatively well-preserved a-wave because of the severe reduction of blood flow to the inner retina. However, the changes in the ERGs do sometimes not correspond with the VA or visual field because the RGC function, which is vulnerable to the ischemia, is not reflected in the ERGs [7].

The PhNR has been reported to reflect the RGC function and serves as a good indicator of severity of the damage of this retinal layer in several types of retinal diseases [10–15]. Our results showed that: (1) the PhNR is reduced in patients with CRAO, (2) a b/a ratio <1.0 was more frequently observed when the photopic ERG recordings were elicited by long-duration stimuli, (3) the degree of the reduction was correlated with the severity of the ocular ischemia, i.e., the amplitude decreased as the severity increased, and (4) the PhNR of the LF photopic ERG was relatively well preserved in eyes which attained a relatively good visual function following the CRAO.

It is interesting that the b/a ratio of the LF photopic ERGs was <1.0 in many cases following a CRAO (fig. 2), considering that this ERG pattern is not found very often in the mixed rod-cone ERGs [7]. Sieving et al. [19] reported that the b-wave of the photopic ERG elicited by an SF is related to the activity of the on-depolarizing bipolar cells (On-DBC) and the off-hyperpolarizing bipolar cells (Off-HBC). The a-wave originates from the activity of the photoreceptors as well as the Off-HBC. Because a CRAO mainly affects the inner retinal layer, the more frequent observation of b/a ratio <1.0 in the LF photopic ERG, to which the Off-HBC contribution is minimal, might suggest that this negative type ERG reflects pure On-DBC dysfunction. Thus, the On-DBC appears to be more susceptible to the ischemic damage. Further investigation is necessary to clarify this observation because long-duration ERGs are likely to be more negative even in normal eyes.

Our results showed that the d-wave of the long-duration photopic ERGs was not significantly different in the 3 CRAO groups and controls, whereas the b-wave was significantly different (fig. 3). Because the d-wave is complex with contributions from the offset of the b-wave, the recovery of the cone receptor response as well as the contribution from the HBC [23], further investigations to examine each of these factors in experimental primates with CRAO would be interesting.

A previous study on animals showed that the correlation of the ERGs and histological changes with the residual retinal circulation variables was not significant [8]. However, in good agreement with the report by Machida et al. [11], who found that the PhNR was the most affected wave following a CRAO, our results showed that the PhNR was significantly reduced in eyes with CRAO. In addition, a significant correlation was found between the amplitude of the PhNR and the angiographically defined severity of the ocular ischemia. In this study, the PhNRs, especially those elicited by long-duration stimuli, were well preserved in eyes which later attained a relatively good visual function. On the other hand, the PhNRs elicited by the SFs did not differentiate eyes with relatively good visual function after CRAO. One explanation for these findings is the influence of the i-wave on the PhNR

in the SF photopic ERG. The i-wave is thought to be associated with the off component [10, 17, 18] and may affect the antecedent PhNR of the SF photopic ERG. The preceding b-wave would tend to offset the following PhNR because the b-wave of the SF photopic ERG reflects the activity of the On-DBC and Off-HBC, whereas the LF photopic ERG reflects primarily the activity of On-DBCs.

It is difficult to conclude which ERG component, a-wave, b-wave, d-wave or PhNR, is most sensitive to retinal ischemia, and which ERG component is most highly correlated with retinal ischemia. The PhNR of the SF photopic ERG was reduced even in group 1 with the minimum severity of circulation disturbances (fig. 4), whereas the a- and b-waves of the SF photopic ERGs and the a-, b- and d-waves and the PhNR of the LF photopic ERG in group 1 were not significantly altered compared to those of the control eyes (fig. 3, 4). These findings suggest that the PhNR of the SF photopic ERG is the most affected and possibly the more sensitive component of the ERG following retinal ischemia. The correlation of the severity of the ocular circulatory disturbance, with respect to the p value, seems strongest for the PhNR elicited by long-duration stimuli ($p = 0.0050$), followed by the b-wave elicited by long-duration stimuli ($p = 0.0062$) and the d-wave elicited by long-duration stimuli ($p = 0.0130$); the PhNR elicited by short-duration stimuli ($p = 0.0498$) had the weakest p value correlation. The degree of the correlation, if any, was strongest for the LF PhNR. However, these conclusions cannot be generalized because our experiments had several limitations such as small sample number, lack of widely accepted quantitative indicators for retinal circulation disturbance and inconsistent treatment for CRAO. Part of these limitations was due to the retrospective nature of the study. It would be interesting to analyze other parameters reflecting retinal circulation such as laser Doppler flowmeter or ocular fundus blood pressure measurements. Our results should therefore be carefully interpreted, but this study still provides clinically useful evidence that the PhNR would be a good indicator for the severity of retinal ischemia in CRAO patients and has potential for predicting visual prognosis. A future prospective study with a larger number of subjects that determines the correlation of each ERG parameter with the visual outcome is needed, especially for the PhNR. These findings should indicate whether the PhNR has a prognostic value or is an indicator for timing or selection of treatment in a routine clinical setting.

Acknowledgement

Support of this study was provided by Researches on Sensory and Communicative Disorders from the Ministry of Health, Labor and Welfare, Japan.

References

1 Yuzurihara D, Iijima H: Visual outcome in central retinal and branch retinal artery occlusion. Jpn J Ophthalmol 2004;48:490–492.
2 Sharma S, Brown GC: Retinal artery obstruction; in Ryan SJ (eds): Retina, ed 4. Philadelphia, Mosby, 2006, pp 1321–1338.
3 Hayreh SS, Kolder HE, Weingeist TA: Central retinal artery occlusion and retinal tolerance time. Ophthalmology 1980;87:75–78.
4 Hayreh SS, Zimmerman MB, Kimura A, Sanon A: Central retinal artery occlusion: Retinal survival time. Exp Eye Res 2004;78:723–736.
5 Carr R, Siegel I: Electrophysiologic aspects of several retinal diseases. Am J Ophthalmol 1964;58:95–107.
6 Hamasaki DI, Kroll AJ: Experimental central retinal artery occlusion: an electrophysiological study. Arch Ophthalmol 1968;80:243–248.
7 Miyake Y: Central retinal artery occlusion; in Miyake Y (ed): Electrodiagnosis of Retinal Diseases. Tokyo, Springer, 2006, pp 181–182.
8 Zhang Y, Cho CH, Atchaneyasakul LO, McFarland T, Appukuttan B, Stout JT: Activation of the mitochondrial apoptotic pathway in a rat model of central retinal artery occlusion. Invest Ophthalmol Vis Sci 2005;46:2133–2139.
9 Viswanathan S, Frishman LJ, Robson JG, Harwerth RS, Smith EL 3rd: The photopic negative response of the macaque electroretinogram: reduction by experimental glaucoma. Invest Ophthalmol Vis Sci 1999;40:1124–1136.
10 Rangaswamy NV, Frishman LJ, Dorotheo EU, Schiffman JS, Bahrani HM, Tang RA: Photopic ERGs in patients with optic neuropathies: comparison with primate ERGs after pharmacologic blockade of inner retina. Invest Ophthalmol Vis Sci 2004;45:3827–3837.
11 Machida S, Gotoh Y, Tanaka M, Tazawa Y: Predominant loss of the photopic negative response in central retinal artery occlusion. Am J Ophthalmol 2004;137:938–940.
12 Chen H, Wu D, Huang S, Yan H: The photopic negative response of the flash electroretinogram in retinal vein occlusion. Doc Ophthalmol 2006;113:53–59.
13 Viswanathan S, Frishman LJ, Robson JG, Walters JW: The photopic negative response of the flash electroretinogram in primary open angle glaucoma. Invest Ophthalmol Vis Sci 2001;42:514–522.
14 Miyata K, Nakamura M, Kondo M, Lin J, Ueno S, Miyake Y, Terasaki H: Reduction of oscillatory potentials and photopic negative response in patients with autosomal dominant optic atrophy with OPA1 mutations. Invest Ophthalmol Vis Sci 2007;48:820–824.

15 Ueno S, Kondo M, Piao CH, Ikenoya K, Miyake Y, Terasaki H: Selective amplitude reduction of the PhNR after macular hole surgery: ganglion cell damage related to ICG-assisted ILM peeling and gas tamponade. Invest Ophthalmol Vis Sci 2006;47:3545–3549.
16 Nagata N: Studies on the photopic ERG of the human retina. Jpn J Ophthalmol 1963;7:96–124.
17 Rufiange M, Rousseau S, Dembinska O, Lachapelle P: Cone-dominated ERG luminance-response function: the Photopic Hill revisited. Doc Ophthalmol 2002;104:231–248.
18 Rosolen SG, Rigaudière F, LeGargasson JF, Chalier C, Rufiange M, Racine J, Joly S, Lachapelle P: Comparing the photopic ERG i-wave in different species. Vet Ophthalmol 2004;7:189–192.
19 Sieving PA, Murayama K, Naarendorp F: Push-pull model of the primate photopic electroretinogram: a role for hyperpolarizing neurons in shaping the b-wave. Vis Neurosci 1994;11:519–532.
20 Feghali J, Jin J, Odom JV: Effect of short-term intraocular pressure elevation on the rabbit electroretinogram. Invest Ophthalmol Vis Sci 1991;32:2184–2189.
21 Johnson M, Drum B, Quigley HA: Pattern-evoked potential and optic nerve fiber loss in monocular laser-induced glaucoma. Invest Ophthalmol Vis Sci 1989;30:897–907.
22 Matsumoto H, Matsumoto CS, Nagata M, Nakatsuka K: Emergency treatment of simultaneous occlusion of central retinal artery and vein (in Japanese). Jpn J Clin Ophthalmol Rinsho Ganka 2005;59:923–927.
23 Ueno S, Kondo M, Ueno M, Miyata K, Terasaki H, Miyake Y: Contribution of retinal neurons to d-wave of primate photopic electroretinograms. Vision Res 2006;46:658–664.

Original Paper

Ophthalmologica

Ophthalmologica 2010;224:103–108
DOI: 10.1159/000235858

Received: October 17, 2008
Accepted after revision: December 11, 2008
Published online: September 1, 2009

Mechanism of Visual Sensations Experienced during Pars Plana Vitrectomy under Retrobulbar Anesthesia

Eiko Sugisaka[a] Kei Shinoda[a, c] Ronaldo Yuiti Sano[b] Susumu Ishida[a]
Yutaka Imamura[a] Yoko Ozawa[a] Hajime Shinoda[a] Kotaro Suzuki[a]
Kazuo Tsubota[a] Makoto Inoue[a, b]

[a]Department of Ophthalmology, Keio University School of Medicine, [b]Kyorin Eye Center, Kyorin University School of Medicine, Tokyo, [c]Department of Ophthalmology, Teikyo University Faculty of Medicine, Oita, Japan

Key Words
Visual experience · Pars plana vitrectomy · Entoptic phenomenon · Retrobulbar anesthesia

Abstract
Purpose: To investigate the visual sensations experienced by patients during vitrectomy under retrobulbar anesthesia. ***Methods:*** 30 men and 45 women with a mean age of 65.3 ± 10.6 years underwent vitrectomy under retrobulbar anesthesia for macular disease. 28 eyes had an idiopathic epiretinal membrane, 13 had an idiopathic macular hole, 32 had macular edema (17 diabetic retinopathy and 15 retinal vein occlusion), and 2 had submacular hemorrhage. 49 patients with nonmacular disease underwent similar vitrectomy procedures and were used for comparison. An interview was conducted with the patient about his/her visual sensations during and within 3 h of the vitrectomy. ***Results:*** 70 (93.3%) of the patients reported seeing lights, 53 (70.7%) reported seeing colors, and 48 (64.0%) reported seeing movements or moving objects. Of the patients who reported seeing movements or moving objects, 44 (58.7%) reported seeing surgical instruments, and 5 (6.7%) saw the surgeon's fingers or hands. Patients with macular diseases tended to report more visual sensations than patients with nonmacular diseases. The patients' description and drawings appeared to arise mainly from the shadows cast by the intravitreal objects, and some patients perceived highly accurate details including the movements and color of the objects. ***Conclusions:*** Visual sensations are experienced by approximately 90% of the patients, and there may be a common mechanism by which patients perceive the intravitreal objects that are not focused on by the retina through the eye's optical system.

Introduction

The visual sensations experienced by patients during vitreous surgery have been described [1–4]. An investigation of 101 patients who underwent pars plana vitrectomy for different vitreoretinal pathologies revealed that light was seen in 90.1%, one or more colors in 72.3%, and movements or moving objects in 56.4% [4]. These observations were similar to earlier reports on the visual sensations experienced by patients during cataract surgery [5–7]. However, one of the differences in the visual sensations reported by patients undergoing cataract and vitreous surgeries was that patients who had vitrectomy

KARGER

Fax +41 61 306 12 34
E-Mail karger@karger.ch
www.karger.com

0030–3755/10/2242–0103$26.00/0

Accessible online at:
www.karger.com/oph

Kei Shinoda, MD
Department of Ophthalmology, Teikyo University Faculty of Medicine
2-11-1 Kaga, Itabashi-ku, Tokyo, 173-8606 (Japan)
Tel. +81 3 3964 1211, ext. 33706, Fax +81 3 3964 1102, E-Mail shinodak@med.oita-u.ac.jp

Table 1. Patient demographics and frequency of patients who experienced various visual sensations during pars plana vitrectomy

	Macular disease				
	macular hole	epiretinal membrane	submacular hemorrhage	macular edema[1]	total
Eyes	13	28	2	32	75
Age, years	67.5 ± 11.4	65.6 ± 9.33	85–68	63.5 ± 11.2	65.3 ± 10.6
Gender (male:female)	3:10	11:17	0:2	16:16	30:45
Preoperative visual acuity (median)	0.1–0.7 (0.2)	0.1–1.0 (0.4)	0.06–0.1 (0.08)	0.06–0.8 (0.2)	0.06–1.0 (0.3)
Visual sensation					
Light	12 (92.3)	27 (96.4)	2 (100)	29 (90.6)	70 (93.3)
Color	10 (76.9)	22 (78.6)	1 (50)	20 (62.5)	53 (70.7)
Moving object	9	18	1	20	48
Instrument	8 (61.5)	17 (60.7)	0	19 (59.4)	44 (58.7)
Vitreous	0 (0)	2 (7.1)	0	5 (15.6)	7 (9.3)
TA particles	7 (53.8)	6/23 (26.1)*	1 (50)	15 (46.9)	29/70 (41.4)
Membranes	3 (23.1)	9 (32.1)	0	5/29 (17.2)	17/72 (18.1)
Others	3 (23.1)	3 (10.7)	0	3 (9.4)	9 (12.0)

Data in columns under Visual sensation and Moving object are presented as number of eyes (%), except for the values indicated by asterisks where the procedure was performed only in selected eyes (the denominator shows the number of eyes). PDR = Proliferative diabetic retinopathy; VH = vitreous hemorrhage; RRD = rhegmatogenous retinal detachment; PVR = proliferative vitreoretinopathy; HM = hand movement; SL = sense of light.

described detailed features of the intraocular objects; forceps, scissors, cutter, crystals of triamcinolone acetonide (TA), and surgical instruments [3, 4].

The purpose of this study was to determine the mechanism causing the visual sensations in patients undergoing vitreous surgery. To accomplish this, we asked patients, especially patients with macular disease, to draw what they experienced. The drawings were made on a fundus picture. An analysis on the patients' drawings provided important evidence on the mechanism of the patients' perceptions. We present more detailed description by several individual patients which could be obtained by asking about their drawings on the fundus photograph. And we discuss the mechanism of this phenomenon.

Patients and Methods

Seventy-five patients with macular localized disease (macular disease) who had pars plana vitrectomy between February 2005 and June 2007 were studied. The visual experiences of these patients were compared with those obtained from 49 patients with nonmacular localized diseases (nonmacular disease) who underwent the same surgical procedures. Part of the group was included in the previous study [4], and 12 patients with macular disease and 11 with nonmacular disease were added. The procedures used conformed to the tenets of the Declaration of Helsinki, and informed consent was obtained after explaining the procedures to each participant. A regional ethics committee approval was not required for this study.

The patients were interviewed during and within 3 h of the vitrectomy concerning their visual experiences during the vitrectomy. Each patient was asked very similar questions during each surgical procedure (online suppl. table 1, for all online supplementary material, see www.karger.com/doi/10.1159/000235858). Patients were also asked to draw their perception on their preoperative fundus picture. Each patient underwent eye surgery for the first time, and the surgery was performed under retrobulbar anesthesia with 5.6 ± 2.5 ml of 2% lidocaine hydrochloride (AstraZeneca Pharma, Bangalore, India). The patients were also premedicated with 2 mg of diazepam, a benzodiazepine, unless there was a contraindication for its use.

Intraoperative observation was performed mostly with an operating microscope (Zeiss CS, Carl Zeiss, Meditec, Tokyo, Japan) with coaxial illumination by multiple surgeons (M.I., K.S., H.S., S.I., Y.I., K.S., Y.O.). The nonoperated eye was carefully covered and draped, and it is highly unlikely that the patient could see anything with this eye. The light from the microscope was usually turned off during the procedures on the posterior segment, unless otherwise indicated. Instead, endoillumination delivered by a fiber optic light source was used, and the level was kept constant throughout the operation. Special attention was paid to keep the intraocular pressure constant at 30 mm Hg by controlling the

Nonmacular disease					p value (totals)
PDR VH	RRD[2]	PVR	miscellaneous[3]	total	
18	20	4	7	49	
52.2 ± 9.83	60.5 ± 10.8	52.3 ± 17.6	65.4 ± 15.6	57.4 ± 12.5	0.0003
12:6	15:5	3:1	7:0	37:12	0.0001
HM–0.6 (0.055)	HM–1.2 (0.15)	HM–0.07[4]	SL–0.5 (0.1)	SL–1.2 (0.07)	0.0135
15 (83.3)	15 (75.0)	3 (75.0)	5 (71.4)	38 (77.6)	0.0104
12 (66.7)	14 (70.0)	1 (25.0)	5 (71.4)	32 (65.3)	0.5297
11	6	0	3	20	
11 (61.1)	6 (30.0)	0 (0)	3 (42.9)	20 (40.8)	0.0518
7 (38.9)	1 (5.0)	0 (0)	0	8 (16.3)	0.243
8 (44.4)	4 (20.0)	0 (0)	1/5 (20)	13/47 (27.7)	0.128
1/11 (9.1)*	0/10 (0)*	0 (0)	0	1/22 (4.55)	0.0624[5]
3 (16.7)	1 (7.7)	0 (0)	0	4 (8.2)	0.4954

[1] Macular edema due to branch retinal vein occlusion in 15 eyes and to diabetic retinopathy in 17 eyes. [2] In six eyes the macula was not involved, and in the other 14 eyes the macula was detached. [3] Multifocal posterior pigment epitheliopathy in one eye, central retinal artery occlusion in one eye, Terson syndrome in one eye, traumatic vitreous hemorrhage in one eye, vitreous hemorrhage due to branch retinal vein occlusion in one eye, intraocular lens dislocation in one eye, asteroid hyalosis in one eye. [4] Visual acuity in four eyes were HM, HM counting finger, and 0.07. [5] Fisher's exact probability test.

height of the bottle for intraocular irrigation (BSS plus®). The BSS plus used had a temperature of 25–27°C.

The surgical procedures were about the same for all eyes and consisted of creation of sclerotomies for three ports, core vitrectomy with a vitreous cutter under endoillumination, intravitreal injection of TA, removal of the epiretinal membrane and/or internal limited membrane, fluid/air exchange, and endolaser photocoagulation. Phacoemulsification and intraocular lens implantation were performed before the vitrectomy in 46 eyes.

The questions were selected to provide information of the visual sensations during different phases of the surgery. The intraoperative questioning was done mainly during the procedures on the posterior segment. The patient's description, preoperative visual acuity, and vitreoretinal disease were analyzed. Statistical comparison between two groups (macular disease vs. nonmacular disease) was made by t tests for patients' age and visual acuity, and by the χ^2 test or Fisher's exact probability test for patients' gender and the incidence of patients who perceived each type of visual sensation. The statistical significance was set at 0.05.

Results

The demographics of the patients and the visual sensations reported by each patient with the different types of macular disease are presented in table 1. There was no obvious difference in the incidence of the type of sensation for the different vitreoretinal pathologies. Seventy (93.3%) patients reported seeing lights, 53 (70.7%) reported seeing colors, and 48 (64.0%) reported seeing movements or moving objects. Of the patients who reported seeing movements or moving objects, 44 (58.7%) reported seeing surgical instruments and 5 (6.7%) saw the surgeon's fingers or hands.

The visual sensations of patients with macular disease were compared with those reported by patients with nonmacular disease (table 1). The type of moving objects perceived was diverse (table 2). No significant difference was found in the incidence of visual sensations between macular disease and nonmacular disease except for light sensations, where the incidence was significantly higher in patients with macular diseases.

In general, patients who saw rod-shaped structures reported that the object entered the field from the left-inferior side and moved to the center of the field. Usually, only one object was seen on the left side of the visual field when an instrument was inserted from the right sclerotomy site and the endoillumination probe was inserted from the left sclerotomy site. When the surgeon inserted a vitreous cutter or forceps from the left sclerotomy site and an endoillumination probe from the right sclerotomy

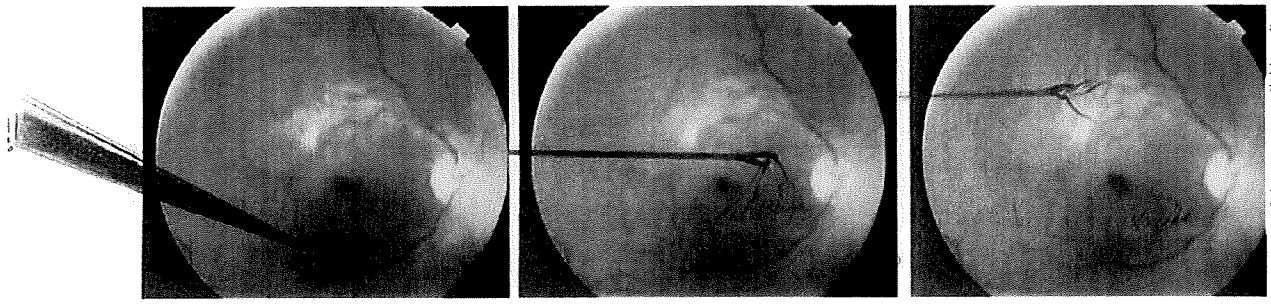

Color version available online

Fig. 1. Picture drawn by a 55-year-old woman who underwent vitrectomy for an epiretinal membrane in the right eye under retrobulbar anesthesia. The drawing shows the patient's visual experience during membrane peeling procedure. What the patient reported is quoted in the text. This drawing shows very clearly that the membrane was picked by the vitreous forceps and peeled off.

Table 2. Details of the visual sensations described by patients who underwent vitrectomy under retrobulbar anesthesia

	Macular diseases		Nonmacular diseases		p value
	eyes	%	eyes	%	
Core vitrectomy or TA injection (n = 124)	75		49		
A stick	36	48.0	18	36.7	0.2161
A small port at the tip of the stick[1]	13	17.3	4	8.2	0.1467
Membrane peeling (n = 94)	72		22		
A stick	26	36.1	6	27.3	0.4439
Shape of the tip of the stick[2]	22	30.5	5	22.7	0.4776
Membrane was peeled off	17	23.6	1	4.6	0.0624[3]

[1] Patients described that snowflake-like materials were aspirated into a small port at the tip of the stick. Some patients reported seeing the blades of the vitreous cutter open and close, and the aspiration of blood or vitreous gel with TA particle through the cannula or vitreous cutter.
[2] Most patients described that the tip looked like the pincette or scissors.
[3] Fisher's exact probability test.

site, the patient reported seeing the object entering from the right.

Some patients underwent pars plana vitrectomy with a fiber optic-free bimanual vitrectomy system in which the illumination was obtained from the microscopic light [8]. Such patients reported seeing two rod-shaped objects entering the center of the visual field from both sides, while the instrument seen on the right side disappeared immediately after the microscope was turned off.

Interestingly, some patients reported seeing the blades of the vitreous cutter opening and closing, and the aspiration of blood or vitreous gel with TA particles through the cannula or vitreous cutter. In addition, some of the patients reported perceiving hemorrhages as red. One patient reported that the instrument in the vitreous cavity was silver, and another patient described it as gold. Patients with a vitreous hemorrhage often said that brown or red swirling gel was seen during the core vitrectomy.

Representative illustrations sketched by a patient on a fundus picture are shown in figure 1. The drawings were made by a 55-year-old woman who underwent vitrectomy for an epiretinal membrane in the right eye. She stated: 'At first I heard click, click in total darkness, and just after the sound stopped, the visual field turned orange and I saw vessels. I saw a stick-like object at the bottom of the eye that was moving approximately 5 mm from the front to the rear. The upper part of the stick looked thick-